Int. J. Advanced Design and Manufacturing Technology, 2024, Vol. 17, No. 1, pp. 29-38

DOI: 10.30486/ADMT.1403.873757 ISSN: 2252-0406 https:// sanad.iau.ir/journal/adm

Numerical and Experimental Investigation of Natural Frequency and Damping Coefficient of Flexible Cellular Lattice Structures

Amir Hosein Samimi, Mohammad Reza Karamooz-Ravari*, Reza Dehghani
Faculty of Mechanical and Materials Engineering
Graduate University of Advanced Technology, Iran
E-mail: amirhshs73@gmail.com, m.karamooz@kgut.ac.ir, r.dehghani@kgut.ac.ir
*Corresponding author

Received: 11 June 2023, Revised: 26 August 2023, Accepted: 10 October 2023

Abstract: Cellular lattice structures encompass a class of metamaterials characterized by the arrangement of interconnected struts and/or plates, offering an adaptable microstructure that enables a broad range of property control. These structures have garnered significant attention for their distinctive properties and have found widespread application across industries such as aerospace, medical, pharmaceutical, automotive, defense, and safety. This study seeks to explore the impact of geometric parameters on the natural frequency and damping coefficient of cellular lattice structures. Samples featuring BCC and OCTET architectures with varying porosities were initially produced using fused deposition modeling (FDM). Subsequently, both experimental and numerical analyses were conducted to assess the first natural frequency and damping coefficient of these materials. Comparison of the numerically obtained results with experimental data revealed a strong agreement. The findings indicate that, for both BCC and OCTET lattices, an increase in porosity is associated with a decrease in both natural frequency and damping coefficient.

Keywords: Finite Element, Lattice Structures, Natural Frequency, Vibration

Biographical notes: Amir Hosein Samimi received his MSc in Mechanical Engineering from Graduate University of Technology, Kerman, Iran, in 2021. **Mohammad Reza Karamooz-Ravari** and **Reza Dehghani** received their PhD in Mechanical Engineering from Isfahan University of Technology (IUT), Isfahan, Iran, in 2015 and 2010, respectively. They are currently associate professors at the Graduate University of Advanced Technology, Kerman, Iran, in the field of additive manufacturing and vibrations, respectively.

Research paper

1 INTRODUCTION

Cellular materials refer to a group of materials that consist of a network of struts and/or plates in three-dimensional space. These materials provide special properties such as high energy absorption, high strength-to-weight ratio, low heat transfer (thermal insulation), low relative density, high sound absorption capability, and low weight [1-2]. Cellular materials can be classified into two groups, including lattice structures and porous materials. In contrast to porous materials, cellular lattice structures have regular structures so that their mechanical properties are highly controllable. Due to their unique properties, these materials have found many applications in various industries, including pharmaceuticals, military, and aerospace [3].

Vibration of mechanical systems is one of the most important causes of failure that might have irreversible effects. In examining the vibrational response of a system, natural frequency is of great importance. The natural frequency of a system depends mainly on its modulus of elasticity, density, and geometry. Accordingly, in order to change the natural frequency of a desired part, its geometry and/or material might be changed. However, in most cases, it is not possible to change the geometry of the part due to the limitations and application constraints. On the other hand, since the modulus of elasticity-to-density ratio of many metals is almost identical, changing the bulk material would not lead to favorable results. Given the above, the use of cellular materials, whose modulus of elasticity and density can be changed and adjusted, is a good option for controlling the vibration response of mechanical systems [4-6].

When human body is exposed to the vibrations of a machine, it can suffer from serious damages to the joints and brain. Accordingly, reducing the amplitude of vibrations, imposed on the occupants of a vehicle, can be very important [7]. Lattice structures are good choices to reduce transmitted vibrations so that it is important to study their vibrational behavior, i.e., natural frequency, mode shapes, and damping coefficient, which might be obtained using the modal analysis. Modal analysis is a method for determining dynamic properties of a structure subjected to dynamic loads. It can be utilized as a tool for determining natural frequency, damping response, and mode shapes, known as modal parameters, as a mathematical function called Frequency Response Function (FRF) [8-10].

Several experimental, numerical, and theoretical studies have been performed in order to obtain the aforementioned modal parameters. Using the definition of joint stiffening element, Dong and Zhao [11] investigated the effect of these joints on the stiffness of the lattice structures made by additive manufacturing and found that the stiffness of the model considering these connections is closer to the experimental results compared to those without these considerations. Kim et al. [12] investigated the effect of debonding embedded between the face-layer laminates and the honeycomb core on the stiffness and natural frequency of sandwich honeycomb beams. Their studies showed that by increasing debonding, the natural frequency decreases. Lou et al. [13] studied the free vibration of sandwich beams under several typical boundary conditions. They also examined the effects of material properties and geometric parameters on natural frequencies. Monkova et al. [14] investigated the effect of cell size and volume ratio on the damping and compression properties of BCC lattice structure made of ABS polymer. The obtained results show that the stiffness and frequency increase with increasing cell thickness.

To enhance the mechanical vibration isolation properties of a machine frame, Syam et al. [6] presented the design, analysis and experimental verification of strut-based lattice structures. They found that a trade-off needs to be made between the frame's natural frequency and its compressive strength in order to achieve high efficiency of vibration isolation. Niu et al. [15] proposed a two scale optimization method in order to find the optimal configuration of cellular lattice structures with maximum structural fundamental frequency. Lopatin et al. [16] theoretically studied the vibrational behavior and frequency response of composite lattice cylindrical shells under clamped-free boundary conditions. Using homogenization approach, Lou et al. [17] modeled a sandwich structure with a pyramidal truss core made of stainless steel under simply-supported boundary condition and investigated the effect of length, radius and inclination angle of the struts on the frequency response of the structure.

By combining the Euler–Bernoulli and Timoshenko beam theories, Xu et al. [18] studied the effects of geometrical and material parameters on the natural frequency of composite sandwich beams with lattice truss core. The effect of the strength of the cellular lattices produced by additive manufacturing technology on their vibration responses was performed by Azmi et al. [19]. They found that the stiffer the lattice is, the higher the frequency would be. Using a combined design and optimization method, Anderson et al. [20] studied the effect of structural irregularities on the fundamental frequency in order to maximize the first eigenfrequency. Utilizing Timoshenko beam elements, Samimi et al. [7] investigated the effects of dimensional inaccuracies, which is an intrinsic characteristic of additive manufacturing of cellular lattice structures, on their natural frequency.

Braun et al. [21] used numerical simulations to assess the effect of the damage percentage, cell type, cell size, and material on the frequency and modal responses of the sandwich plates. Scalzo et al. [4] investigated the

influence of the experimental setup of modal analysis on the modal parameters of different SLM AISI 316L lattice structures. In another work [5], they used experimental and numerical investigations in order to assess the dynamic behavior of lattice structures in the medium-high frequency range. Yi et al. [22] used the finite element approach to calculate the axial vibration characteristics of pyramid lattice cylindrical structure and assessed the effects of different parameters on its damping capability.

Tempelman et al. [23] studied the broadband vibration absorption characteristics of three different latices, i.e., simple-cubic, diamond and octet-truss, using experimental and theoretical methods. Wei et al. [24] carried out finite element numerical simulation and modal testing of the dynamic damping performance of steel-based Kelvin lattice structures fabricated by indirect additive manufacturing. They found that the natural frequency and damping ratio might be regulated by changing the lattice porosity. Zhang et al. [25] investigated the frequency response and damping ratio of IWP-type triply periodic minimal surfaces (TPMS) lattice structures by dynamic vibration transfer rate tests. They concluded that the stiffness and inherent frequency of the lattice structure are directly and inversely proportional to the volume fraction and the cell size, respectively. Liu et al. [26] proposed a multiscale topology optimization framework for maximizing the natural frequency of multi-morphology lattice structures (MMLSs). Multi-morphology lattice unit cells with smooth characteristics were achieved using the Kriging-assisted morphological post-process and sigmoid function-based hybrid transition strategy.

Since the flexible TPU polymers have high intrinsic damping capability, TPU cellular lattice structures would be good candidates for vibration isolations. In this paper, two different cellular lattice structures, i.e., BCC and OCTET, with different values of porosity are additively manufactured using TPU flexible polymers. Then, the first natural frequency as well as damping coefficient is obtained by experimental measurements. In addition, a solid finite element model is developed in order to predict the above-mentioned modal parameters. The obtained results show a good agreement between experimental and numerical findings. Moreover, it is concluded that the natural frequency as well as damping coefficient decreases as the porosity of the structures increases.

2 MATERIALS AND METHODS

This section begins with a brief overview of the lattices under consideration, followed by an explanation of how the samples were fabricated. It then introduces the approach used for setting up and conducting the experiments, as well as the finite element modeling and three-dimensional representation of the samples. The section concludes with a comprehensive explanation of the methods used to estimate the damping coefficient of the samples, incorporating both numerical and experimental data.

In this paper, two different cellular lattice structures, i.e., BCC and OCTET, are chosen for experimental and numerical analysis. Figure 1 (a) and (b) respectively demonstrate the schematic representation of the unit cells corresponding to BCC and OCTET lattice structures.

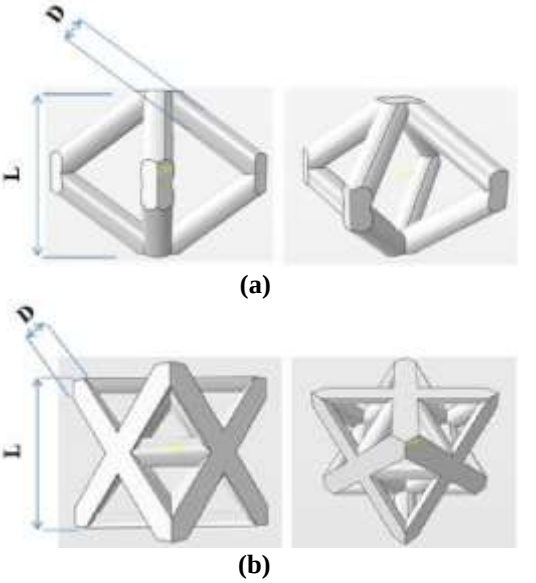

Fig. 1 Schematic representation of the unit cell corresponding to the lattice structure: (a): BCC, and (b): OCTET. Here D is the struts' diameter and L is the unit cell size.

As can be seen, the BCC unit cell contains 8 diagonal struts connecting 6 vertices while the OCTET unit cell is comprised of 14 vertices connected by 36 struts. Considering *s* as the number of struts, and *v* the number of vertices, the Maxwell number, *M*, might be introduced as [27-28]:

$$M = s - 3v + 6 \tag{1}$$

If $M < 0$, the lattice is considered as bending-dominated structure, while for $M \geq 0$, the axial deformation mechanism is the main one so that the lattice is called stretch-dominated. Using Equation (1), the Maxwell number of BCC and OCTET lattices is equal to -4 and 0, respectively. Accordingly, BCC lattice structure is bending-dominated while OCTET is stretch-dominated.

2.1. Sample Fabrication

In this paper, Fused Deposition Modeling (FDM) is used for fabrication purposes. To do so, a three-dimensional model generated through ABAQUS finite element package, is exported as STL format and used as the input of the FDM machine. Quantum 2025 3D printer, manufactured by Persia 3D Printer Company, is utilized to produce the lattices. Using this machine, a part with the dimensions of 20, 20, and 25 cm respectively in directions of x, y, and z-axes, can be fabricated. The utilized process parameters are presented in "Table 1".

Table 1 Process parameters used for fabrication purposes

Parameter	Value	Unit
Initial Layer thickness	0.25	*mm*
Layer height	0.2	*mm*
Shell thickness	0.8	*mm*
Bottom/Top thickness	0.6	*mm*
Fill Density	100	*%*
Print speed	25	*mm/s*
Retraction speed	27	*mm/s*
Travel speed (Nozzle speed)	27	*mm/s*
Printing temperature	200	$^{\circ}C$
Bed temperature	40	$^{\circ}C$

All the samples are fabricated from TPU flexible polymer filaments, produced by YS Company. The filament has the diameter of 1.75 mm, and its operating temperature is in the range of 200 to 245 degrees Celsius. The physical properties of the material that are required for the simulation of frequency response are elastic modulus of 4 *GPa*, density of 1200 Kg/m^3, and Poisson's ratio of 0.47.

Due to the limitations of the utilized machine, the unit cell size, *L*, is supposed to be 17 *mm* and the struts' diameter are chosen in a way that the desired porosity can be obtained. The porosity values of BCC lattices are considered to be 65 and 85 percent, which are related to the strut's diameter of 5 and 3.1 *mm*, and the values of 65 and 75 percent are chosen for OCTET lattice structures, corresponding to the strut's diameter of 3.25 and 2.65 *mm*. Notice that for OCTET lattice structure with a porosity of 85%, the struts' diameter would be about 2 *mm* which cannot be produced with a good quality by the utilized printing machine. Thus, 75% porosity is considered instead of 85%.

2.2. Experimental Measurements

In order to calculate FRF, first, a vibratory excitement is generated in the structure by applying a certain force to a specific point and the vibration response, which is the output-to-input ratio, is measured at another point. To do so, three major steps, including preparing test setup, measuring frequency response by applying excitation force, and data processing must be followed. The excitation force is applied to the structure at a suitable range by various devices such as modal hammer [4], [9], which is equipped with several hammerheads, accelerometer sensor and a handle. Hammerheads are made of different materials such as plastic and steel, each of which is attached to the hammer according to the bulk material of the component being tested. The accelerometer sensor is the most important part of the hammer machine that measures the acceleration of the component being tested and displays it at the outlet. The accelerometer should be firmly attached to the desired part; however, this is not possible in practice which can affect the accuracy of the measurements; so that, the firmer the connection base, the more accurate the result would be. The accuracy of this sensor depends on various factors such as rigidity of the boundaries, air temperature, and humidity [9].

As shown in "Fig 2", the fabricated samples are supposed to be clamped at one end and free at the other. In order to create this type of boundary conditions, Zipper glue is used to attach the samples to a chipboard, and the clipboard to the wall. Since the sensor can be attached to the desired location of the parts using magnets, it is necessary to attach a piece of steel at that site. As shown in "Fig 2", a circle-shaped piece of steel, with the diameter of at least 2.54 cm, which is equal to the loadcell diameter, is glued to the center of the samples for attaching the sensor.

The fundamental frequency and damping coefficient are obtained experimentally using modal analysis. To perform modal analysis and data processing, Vib V4 Pro vibrometer equipped with piezoelectric accelerometer sensor and modal hammer fabricated by Delta Sanat Sharif Company is used. This device could be applied for several types of condition monitoring, including dynamic balance of surfaces, measurement of vibrations and natural frequency, and speed analysis. It is important to note that the cable connected to the hammer should be connected to channel 1 of Vib V4 Pro and loadcell cable should be connected to channel 2. After connecting these two devices, the other end of the loadcell should be connected to the circle-shaped steel attached to the desired structure. Due to the short time interval between the start time of the test and hitting time, the modal hammer is kept close to the component, so that a low impact was done immediately after the test started. In this way, the amplitude was displayed graphically in terms of frequency. Accordingly, damping was obtained using half-power bandwidth method, which will be briefly introduced in the next sections.

2.3. Finite Element Modeling

ABAQUS finite element package is utilized for three-dimensional modeling as well as numerical simulations. To do so, a Python script is developed in order to generate the three-dimensional model of the unit cell of the lattices. The program receives the coordinates of the vertices of the structures, the connection matrix, struts'

diameter (D), and unit cell size (L) to produce the unit cell of the lattices. The unit cell is then repeated along different perpendicular directions to construct the whole structure of concern.

(a)

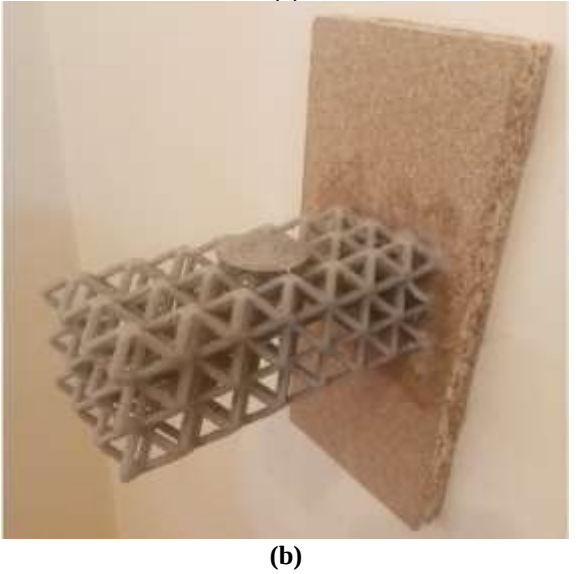

(b)

Fig. 2 Preparing the clamped-free boundary conditions for: (a): OCTET65%, and (b): BCC85%.

The lattices are meshed using 10-node quadratic tetrahedron elements denoted by C3D10 in ABAQUS. A mesh sensitivity analysis is then performed, by reducing the mesh size by a factor of 0.5, until the difference between the natural frequencies of two successive simulations is smaller than 10 percent.
In order to compare the results, the boundary conditions of all the samples are considered to be identical. In this paper, in accordance with the experimental tests, one side of the specimen is completely constrained, so that:

$$U_1 = U_2 = U_3 = 0 \tag{2}$$

Where U_1, U_2, and U_3 are the translational degrees of freedom in the x, y, and z directions, respectively.
Given that natural frequency is the intended output, no applied load is considered. However, impact loading was applied in a short period in damping analysis stage in order to accurately simulate the experimental test of modal analysis. "Table 2", presents how the load was applied during the analysis period.

Table 2 The applied load history during the simulation of damping of the structure

Load Magnitude	Time (s)
0	0.0
0	0.05
1	0.10
0	0.15
0	0.2
0	1

2.4. Frequency and Damping Analysis

This section explains how to determine the intended output and calculate the fundamental frequency and damping, numerically and experimentally.
In order to perform the damping analysis, the subspace solution method is utilized along with the modal dynamic approach to obtain the displacement response of the desired point of the lattice, as shown in "Fig 3".

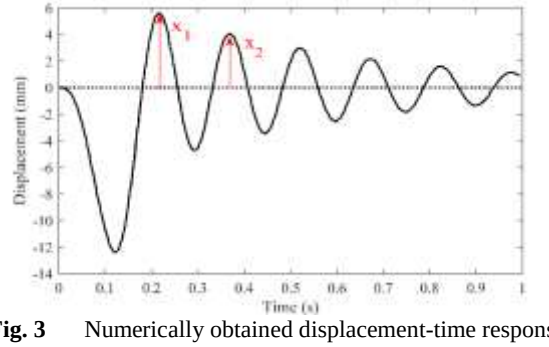

Fig. 3 Numerically obtained displacement-time response.

In this context, the analysis time is defined as 1 second divided into 1000 segments. The greater the number of these segments are, the more accurate the analysis response would be. However, the computation time is drastically depended on the number of these segments.
Damping ratio, ξ, can be calculated considering the two successive peaks of the graph shown in "Fig. 3" and using Equation (3) [10]:

$$\xi = \sqrt{\frac{\delta^2}{\delta^2 + 1}} \tag{3}$$

Where:

$$\delta = \frac{1}{2\pi} \ln\left(\frac{x_i}{x_{i+1}}\right) \quad (4)$$

In which x_i is the displacement at the i-th peak. The data obtained from the experimental test performed by the vibrometer are analyzed in MRS3000 software which can magnify the graphs. The frequency amplitude graph in the software is logarithmic in db. Therefore, the graph was taken out of logarithmic state in order to use half-power bandwidth method. As shown in "Fig. 4", the half-power bandwidth method assumes that the frequency response is approximately symmetric, with respect to vertical axes at natural frequency in the amplitude-frequency graph.

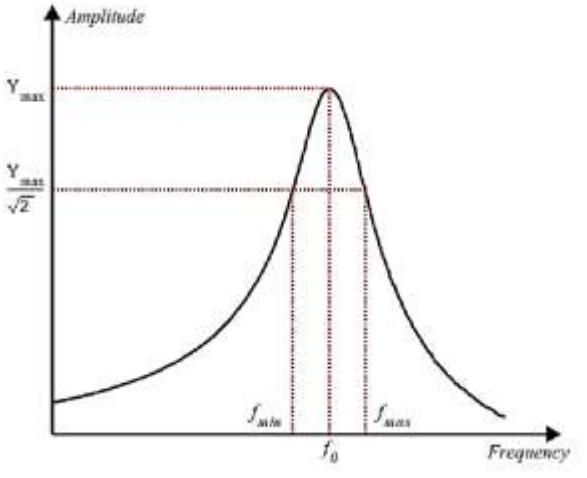

Fig. 4 Schematic representation of half power bandwidth method.

The graph peak indicates the desired frequency and the value corresponding to this point is displayed on the vertical axis as Y_{max}. Then, this value is divided by $\sqrt{2}$ and the obtained value is marked on the vertical axis. Afterwards, a hypothetical line parallel to the horizontal axis is drawn to determine the points colliding with the frequency response graph and the frequencies f_{min} and f_{max} are obtained. The damping ratio can then be determined using the following Equation [20]:

$$\xi = \frac{f_{\max} - f_{\min}}{2 f_0} \quad (5)$$

3 RESULTS AND DISCUSSION

In this section, we begin by presenting the results obtained from frequency analysis, both from numerical simulations and experimental measurements, followed by a discussion on the comparison between these results. Subsequently, we present the findings from the damping analysis, and provide a comparison between the results obtained from numerical simulations and experimental observations.

The experimental and numerical analysis are performed on samples comprised of 3*3*7 cells in 3 orthogonal directions. Each experimental measurement is repeated twice and the average outputs are used for calculations. In the case of finite element modeling, after mesh sensitivity analysis, a mesh size of 8 mm and 12 mm is obtained for the BCC and OCTET cellular lattice structure, respectively. By applying this mesh sizes to the structures, the BCC structure with 65% and 85% porosity, and OCTET structure with 65% and 75% porosity contains respectively 202046, 211735, 234921, and 164939 elements.

3.1. Simulation Results for Fundamental Frequency

"Table 3" presents the simulation results of the first three modes in ABAQUS software for BCC structure with 65% and 85% porosities and OCTET structure with 65% and 75% porosities.

Table 3 Results of frequency analysis for the first 3 modes

Structure Type	Porosity (%)	Mode number	Diameter (mm)	Natural frequency (HZ)
BCC	65	1	5	12.27
BCC	65	2	5	12.53
BCC	65	3	5	45.90
BCC	85	1	3.1	6.6
BCC	85	2	3.1	6.9
BCC	85	3	3.1	24.55
OCTET	65	1	3.25	16.594
OCTET	65	2	3.25	16.597
OCTET	65	3	3.25	45.21
OCTET	75	1	2.65	14.75
OCTET	75	2	2.65	14.76
OCTET	75	3	2.65	41.85

According to the results obtained for the first mode of the structures, it can be concluded that the natural frequency decreased by increasing the structure porosity, the reason for which could be attributed to the reduced stiffness due to the decreased strut diameter. In addition, at the same value of porosity, the fundamental frequency of the OCTET lattices is almost 35% higher than that of BCC structure.

3.2. Experimental Results for Fundamental Frequency

Figures 5 and 6 indicate the amplitude at an acceptable bandwidth as a function of frequency for BCC and OCTET cellular lattice structures, respectively. Two tests were taken from each structure, and the average values are reported. Using these two figures, the

fundamental natural frequency is obtained and presented in "Table 4". It can be observed that the numerically obtained results are in good agreement with the experimentally measured ones. The maximum error is about 15.71 percent which is associated with OCTET cellular lattice structure with 75 percent porosity.

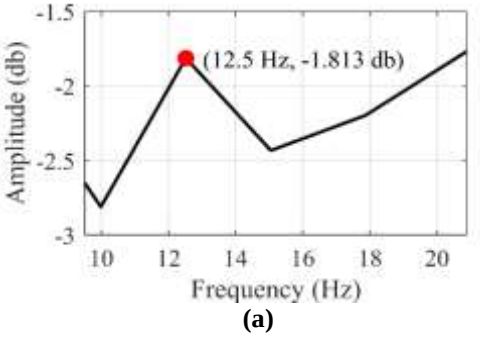

(a)

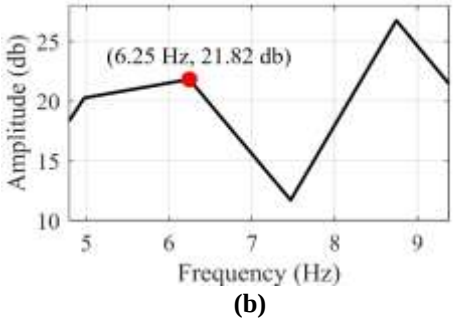

(b)

Fig. 5 The amplitude at an acceptable bandwidth as a function of frequency for BCC cellular lattice structure with: (a): 65% porosity, and (b): 85% porosity.

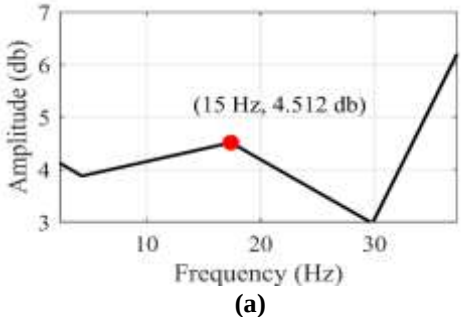

(a)

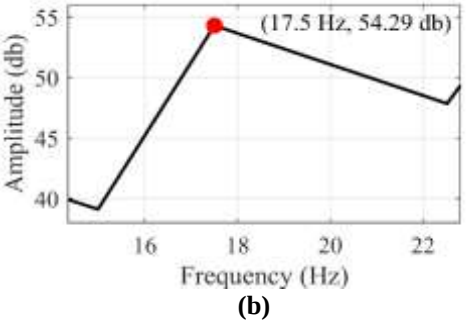

(b)

Fig. 6 The amplitude at an acceptable bandwidth as a function of frequency for OCTET cellular lattice structure with: (a): 65% porosity, and (b): 75% porosity.

Table 4 Comparison of the experimentally (exp) and numerically (FEM) obtained fundamental natural frequency as well as damping coefficient. Here, err stands for the error between the numerical and its corresponding experimental value

Lattice	Porosity (%)	Fundamental frequency (Hz)		Damping coefficient	
		exp	FEM [err %]	exp	FEM [err %]
BCC	65	12.5	12.27 [1.84]	0.1838	0.1958 [6.5]
BCC	85	6.25	6.6 [5.6]	0.45	0.1052 [76]
OCTET	65	15.0	16.59 [9.58]	0.319	0.266 [16.6]
OCTET	75	17.5	14.75 [15.71]	0.2272	0.2112 [7.0]

3.3. Damping Analysis Results

Referring to the results presented in Section 3.2, the damping ratio is calculated and the results for the four structures are given in "Table 4". Given that calibration should be performed in order to obtain numerical damping, an explanation of calibration and how it should be done is provided. Then, results of experimental and numerical tests are presented and compared.

In numerical investigations, either Rayleigh or structural damping might be used to evaluate damping coefficient of the lattices. However, since there is no available source about structural damping as well as damping degree of the utilized bulk material, Rayleigh damping method was employed in which [10]:

$$\xi = \frac{\alpha}{2\omega} + \frac{\beta\omega}{2} \tag{6}$$

In order to calibrate α and β parameters, different logical values are assigned to the parameters and damping coefficient is calculated through amplitude-displacement graph as mentioned earlier. When the calculated value became equal to the experimentally obtained damping coefficient for BCC structure with 65% porosity, values of α and β coefficients are considered as the parameters associated with the bulk material. These values are then attributed to the bulk material for all other simulations. Using this approach, α = 0.02 and β = 0.005 are obtained.

Figures 7 to 10 show the displacement at the accelerometer sensor installation site as a function of time for BCC lattice structures with 65 and 85% porosity and OCTET structures with 65 and 75% porosity, respectively. These curves are used to calculate the damping coefficient of the lattices.

The numerically obtained damping coefficient along with the error from experimental findings is calculated

and presented in "Table 4". Comparing these results shows that, except for the BCC structure with 85% porosity, the numerical and experimental results are well consistent.

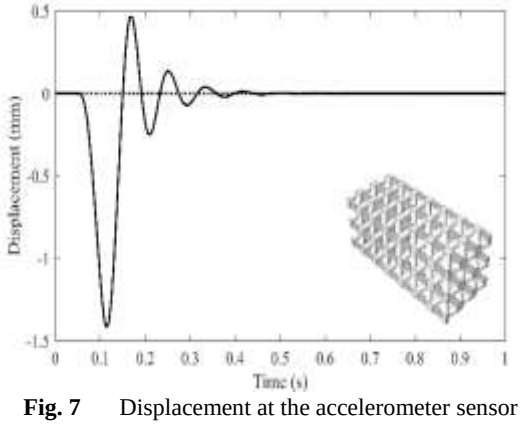

Fig. 7 Displacement at the accelerometer sensor installation site as a function of time for BCC lattice with 65% porosity.

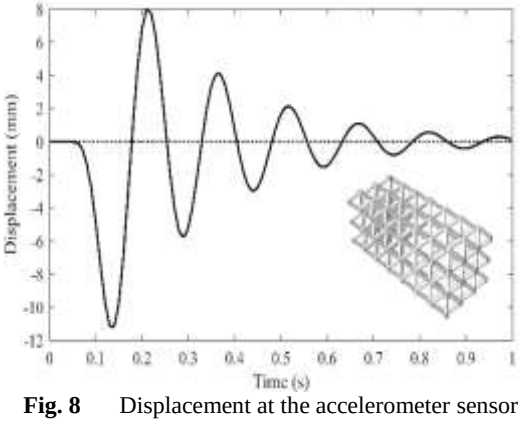

Fig. 8 Displacement at the accelerometer sensor installation site as a function of time for BCC lattice with 85% porosity.

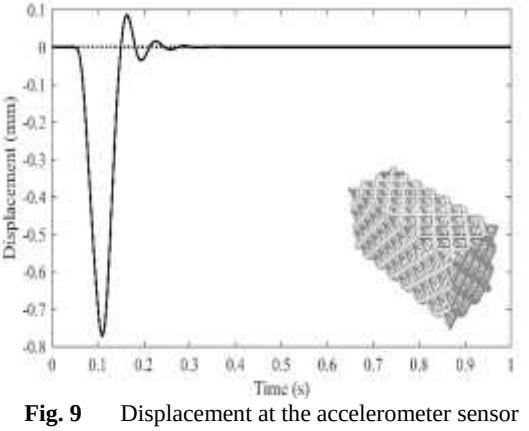

Fig. 9 Displacement at the accelerometer sensor installation site as a function of time for OCTET lattice with 65% porosity.

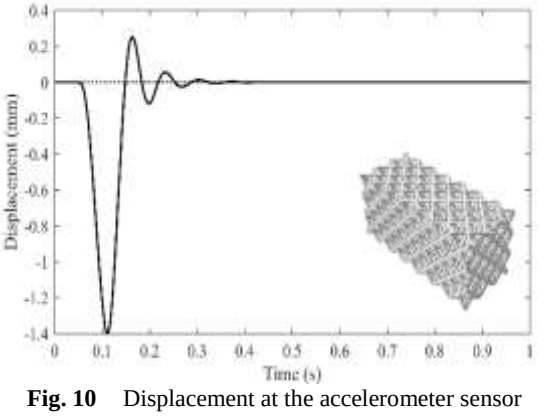

Fig. 10 Displacement at the accelerometer sensor installation site as a function of time for OCTET lattice with 75% porosity.

The reason for the discrepancy of experimental and numerical damping for this structure can be low accuracy of the device for this range of natural frequency and low mass and stiffness of the structure, which causes a lot of vibration in the structure with the slightest impact. In addition, it can be concluded that the damping ratio decreases as the porosity increases. Moreover, the value of damping coefficient of OCTET lattices is 36% higher than the damping coefficient of BCC lattices with the same value of porosity.

4 CONCLUSIONS

This paper presents a comprehensive examination of the natural frequency and damping coefficient of two cellular lattice structures, namely BCC and OCTET, through both numerical simulations and experimental investigations. The results demonstrate a strong correspondence between the numerical and experimental data, with the largest frequency error occurring in the OCTET cellular lattice structure with 75% porosity, amounting to 15.7%. The study reveals that as the porosity of the structure increases, both the natural frequency and damping coefficient decrease, attributed to the reduced stiffness resulting from the decrease in strut diameter. Furthermore, the OCTET structure exhibits higher natural frequency and damping coefficient compared to the BCC structure.

REFERENCES

[1] Ashby, M. F., et al., Metal Foams: A Design Guide, Elsevier, 2000.

[2] Banhart, J., Manufacturing Routes for Metallic Foams, Jom, Vol. 52, No. 12, 2000, pp. 22-27.

[3] Meisel, N. A., Williams, C. B., and Druschitz, A., Lightweight Metal Cellular Structures Via Indirect 3D

Printing and Casting. in 2012 International Solid Freeform Fabrication Symposium, University of Texas at Austin, 2012.

[4] Scalzo, F., Totis, G., and Sortino, M., Influence of the Experimental Setup on the Damping Properties of SLM Lattice Structures. Experimental Mechanics, Vol. 63, No. 1, 2023, pp. 15-28.

[5] Scalzo, F., et al., Experimental Study on The High-Damping Properties of Metallic Lattice Structures Obtained from SLM, Precision Engineering, Vol. 71, 2021, pp. 63-77.

[6] Syam, W. P., et al., Design and Analysis of Strut-Based Lattice Structures for Vibration Isolation, Precision Engineering, Vol. 52, 2018, pp. 494-506.

[7] Samimi, A. H., Karamooz-Ravari, M. R., and Dehghani, R., Investigation of the Effects of Dimensional Inaccuracies on the First Natural Frequency of Cellular Lattice Structures, ADMT Journal, Vol. 15, No. 3, 2022, pp. 109-117.

[8] Døssing, O., Structural Testing: Modal Analysis and Simulation, Brüel & Kjær (Ed.), Vol. 2. 1988.

[9] Brown, D. L., Passing the Torch-Structural Dynamics/Modal Analysis from Here to Sound and Vibration, Vol. 34, No. 1, 2000, pp. 6-7.

[10] Fu, Z. F., He, J., Modal Analysis, Elsevier, 2001.

[11] Dong, G., Zhao, Y. F., Numerical and Experimental Investigation of The Joint Stiffness in Lattice Structures Fabricated by Additive Manufacturing, International Journal of Mechanical Sciences, Vol. 148, 2018, pp. 475-485.

[12] Kim, H. Y., Hwang, W., Effect of Debonding on Natural Frequencies and Frequency Response Functions of Honeycomb Sandwich Beams, Composite Structures, Vol. 55, No. 1, 2002, pp. 51-62.

[13] Lou, J., et al., Free Vibration Analysis of Lattice Sandwich Beams Under Several Typical Boundary Conditions, Acta Mechanica Solida Sinica, Vol. 26, No. 5, 2013, pp. 458-467.

[14] Monkova, K., et al., Mechanical Vibration Damping and Compression Properties of a Lattice Structure, Materials, Vol. 14, No. 6, 2021, pp. 1502.

[15] Niu, B., Yan, J., and Cheng, G., Optimum Structure with Homogeneous Optimum Cellular Material for Maximum Fundamental Frequency, Structural and Multidisciplinary Optimization, Vol. 39, No. 2, 2009, pp. 115-132.

[16] Lopatin, A., Morozov, E., and Shatov, A., An Analytical Expression for Fundamental Frequency of The Composite Lattice Cylindrical Shell with Clamped Edges, Composite Structures, Vol. 141, 2016 pp. 232-239.

[17] Lou, J., Ma, L., and Wu, L. Z., Free Vibration Analysis of Simply Supported Sandwich Beams with Lattice Truss Core, Materials Science and Engineering: B, Vol. 177, No. 19, 2012, pp. 1712-1716.

[18] Xu, M., Qiu, Z., Free Vibration Analysis and Optimization of Composite Lattice Truss Core Sandwich Beams with Interval Parameters. Composite Structures, Vol. 106, 2013, pp. 85-95.

[19] Azmi, M. S., et al. Vibration Analysis of FDM Printed Lattice Structure Bar, In Proceedings of SAKURA Symposium on Mechanical Science and Engineering, 2017.

[20] Andresen, S., Bäger, A., and Hamm, C., Eigenfrequency Maximisation by Using Irregular Lattice Structures, Journal of Sound and Vibration, Vol. 465, 2020, pp. 115027.

[21] Braun, M., vanez, I., and Aranda-Ruiz, J., Numerical Analysis of the Dynamic Frequency Responses of Damaged Micro-Lattice Core Sandwich Plates, The Journal of Strain Analysis for Engineering Design, Vol. 55, No. 1-2, 2020, pp. 31-41.

[22] Yi, R., et al., Axial Elastic Wave Propagation Characteristics of Pyramid Lattice Cylindrical Structure, Chinese Journal of Theoretical and Applied Mechanics, Vol. 54, No. 10, 2022, pp. 2717.

[23] Tempelman, J. R., et al., Experimental Investigations into Broadband Vibration Absorption of Metastructures with Lattice Designs. in ASME 2019 International Design Engineering Technical Conferences and Computers and Information in Engineering Conference, 2019.

[24] Wei, Y., et al., Damping Behaviors of Steel-Based Kelvin Lattice Structures Fabricated by Indirect Additive Manufacture Combining Investment Casting, Smart Materials and Structures, Vol. 29, 2020, pp. 055001.

[25] Zhang, C., et al., Vibration Characteristics of Additive Manufactured IWP-type TPMS Lattice Structures, Composite Structures, Vol. 327, 2024, pp. 117642.

[26] Liu, X., Gao, L., and Xiao, M. Multiscale Topology Optimization Framework for Natural Frequency Maximization of Multi-Morphology Lattice Structures, Composite Structures, Vol. 328, 2024, pp. 117720.

[27] Maconachie, T., et al., SLM Lattice Structures: Properties, Performance, Applications and Challenges, Materials & Design, Vol. 183, 2019, pp. 108137.

[28] Phani, A. S. and Hussein, M. I., Dynamics of Lattice Materials, Wiley, 2017.